Supplementary Information for:

Overall performance improvement of direct-current triboelectric nanogenerator by charge leakage and ternary dielectric evaluation

Qianying Li,[a] Shaoke Fu,[a] Xiaochuan Li,[a] Huilin Chen,[a] Wencong He,[a] Qianxi Yang,[a] Xuemei Zhang,[a] Huake Yang,[a] Dahu Ren,[a] and Yi Xi[a]*

[1] Chongqing Key Laboratory of Soft Condensed Matter Physics and Smart Materials, Department of Applied Physics, School of Chemistry and Chemical Engineering, Chongqing University, Chongqing, 400044, P. R. China.

*Corresponding authors. Email: yxi6@cqu.edu.cn (Y. Xi)

Keywords: DC triboelectric nanogenerator, average power density, material evaluation, low crest factor, charge leakage effect.

Content

Supplementary Figures

Supplementary Tables

Supplementary Notes

Supplementary Figures

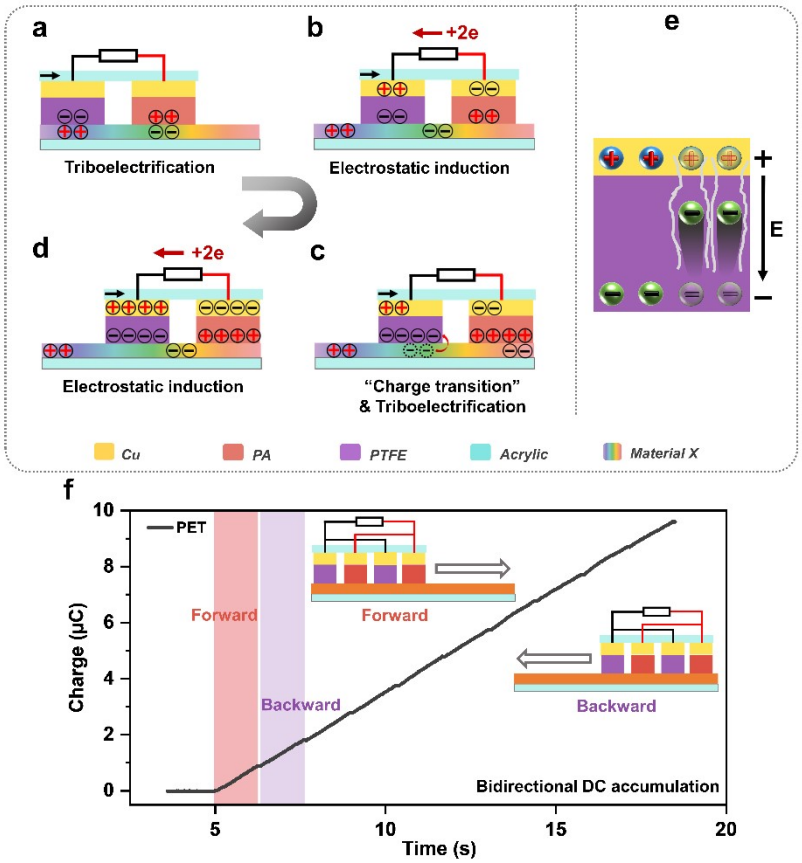

Fig. S1. Working mechanism of the sliding T-DC-TENG. **a-d** Working mechanism of the sliding T-DC-TENG before reaching charge saturation state. **e** Schematic diagram (cross-sectional view) of electrons on the PTFE passing through the film in the form of charge leakage due to the strong electric field. **f** Charge output of the sliding T-DC-TENG with bidirectional DC charge accumulation in reciprocating motions.

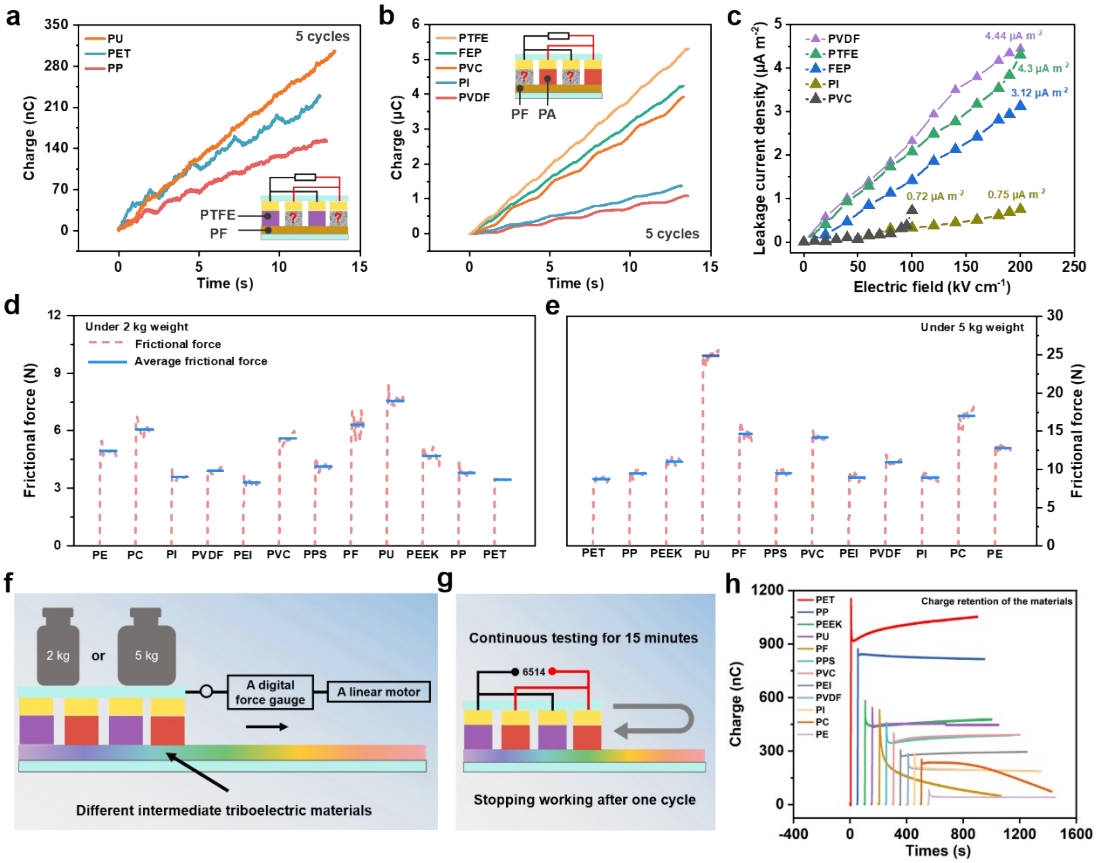

Fig. S2. Properties and test methods of different tribo-layer materials. **a** Raw data plot of DC output charge of 2-unit T-DC-TENG with different electropositive materials (PU, PET, and PP). **b** Raw data plot of DC output charge of 2-unit T-DC-TENG with different electronegative materials (PTFE, FEP, PVC, PI, and PVDF). **c** Leakage current density of the most typical electronegative materials. **d**, **e** Frictional forces and average frictional forces of different intermediate triboelectric materials under the pressure of 2 kg and 5 kg weights. **f** Schematic diagram of testing the frictional force of intermediate triboelectric materials. **g** Schematic diagram for testing the charge retention ability of intermediate triboelectric materials. **h** Raw data plot of charge output of T-DC-TENG with different intermediate triboelectric materials within 15 minutes after one cycle.

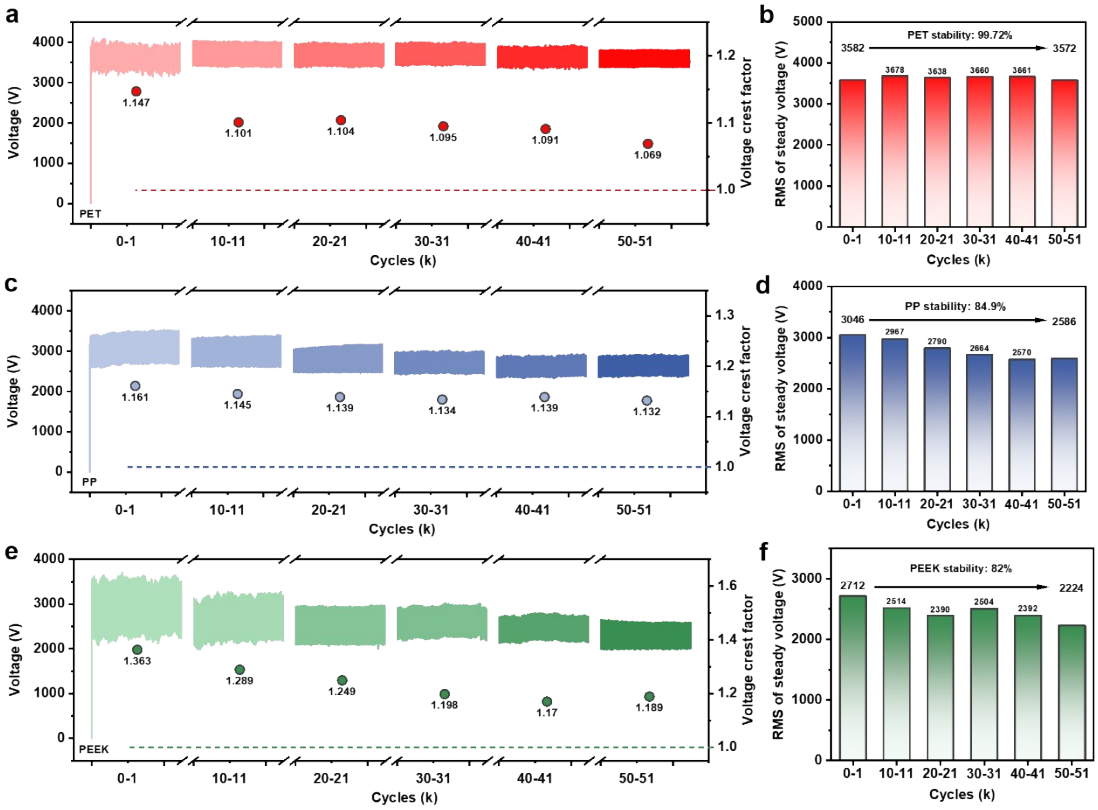

Fig. S3. Stability test of T-DC-TENG with different intermediate triboelectric materials (PET, PP, and PEEK) within 50000 cycles. Voltage output, RMS of steady voltage, and voltage crest factor of T-DC-TENG with different intermediate triboelectric materials (**a**, **b** PET, **c**, **d** PP, and **e**, **f** PEEK) per 10000 cycles.

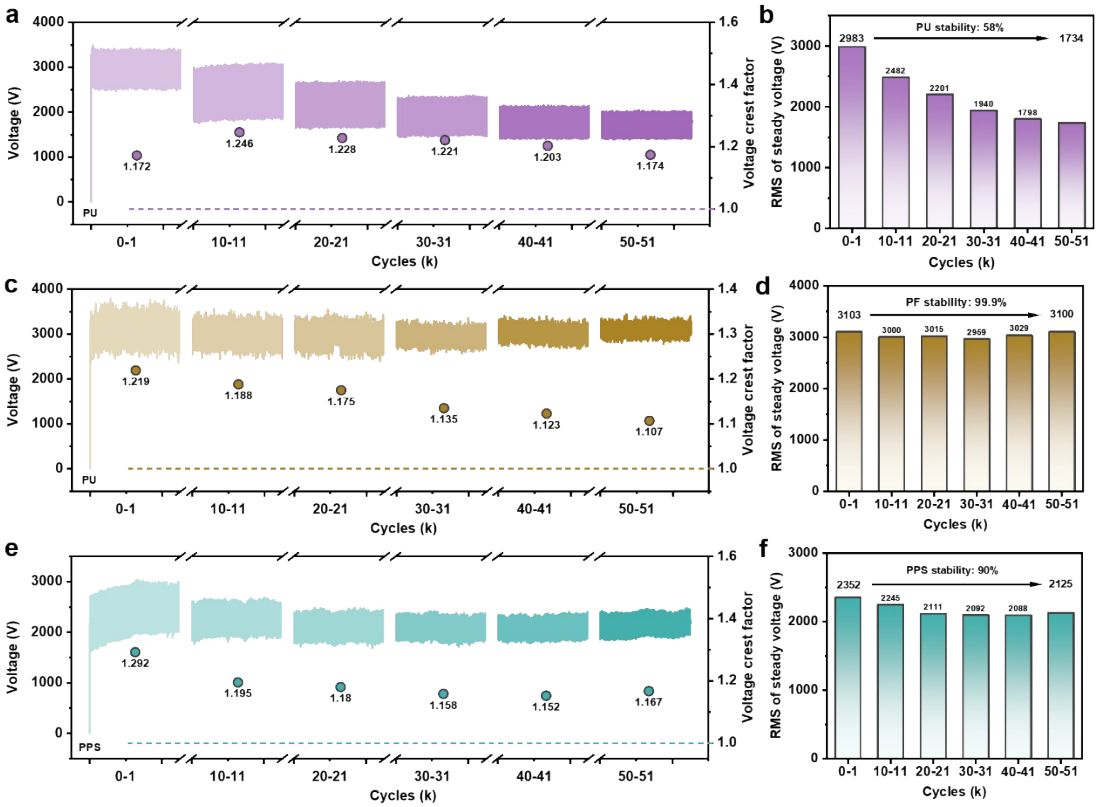

Fig. S4. Stability test of T-DC-TENG with different intermediate triboelectric materials (PU, PF, and PPS) within 50000 cycles. Voltage output, RMS of steady voltage, and voltage crest factor of T-DC-TENG with different intermediate triboelectric materials (**a**, **b** PU, **c**, **d** PF, and **e**, **f** PPS) per 10000 cycles.

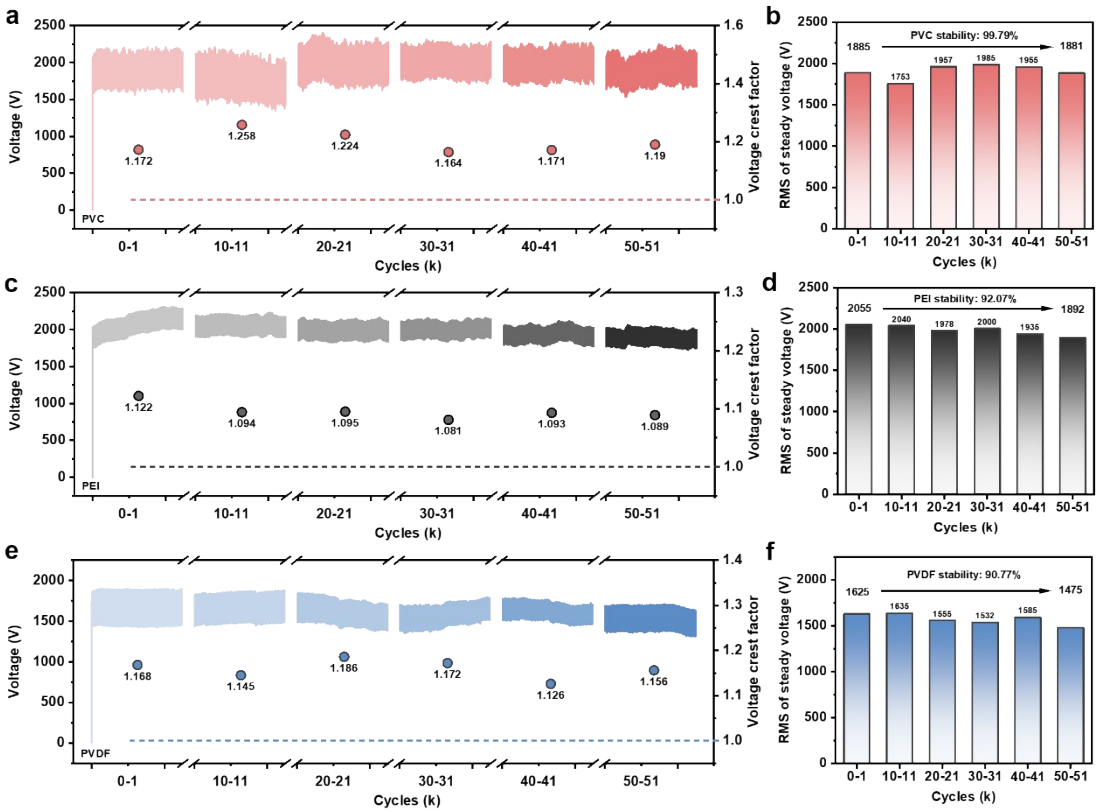

Fig. S5. Stability test of T-DC-TENG with different intermediate triboelectric materials (PVC, PEI, and PVDF) within 50000 cycles. Voltage output, RMS of steady voltage, and voltage crest factor of T-DC-TENG with different intermediate triboelectric materials (**a**, **b** PVC, **c**, **d** PEI, and **e**, **f** PVDF) per 10000 cycles.

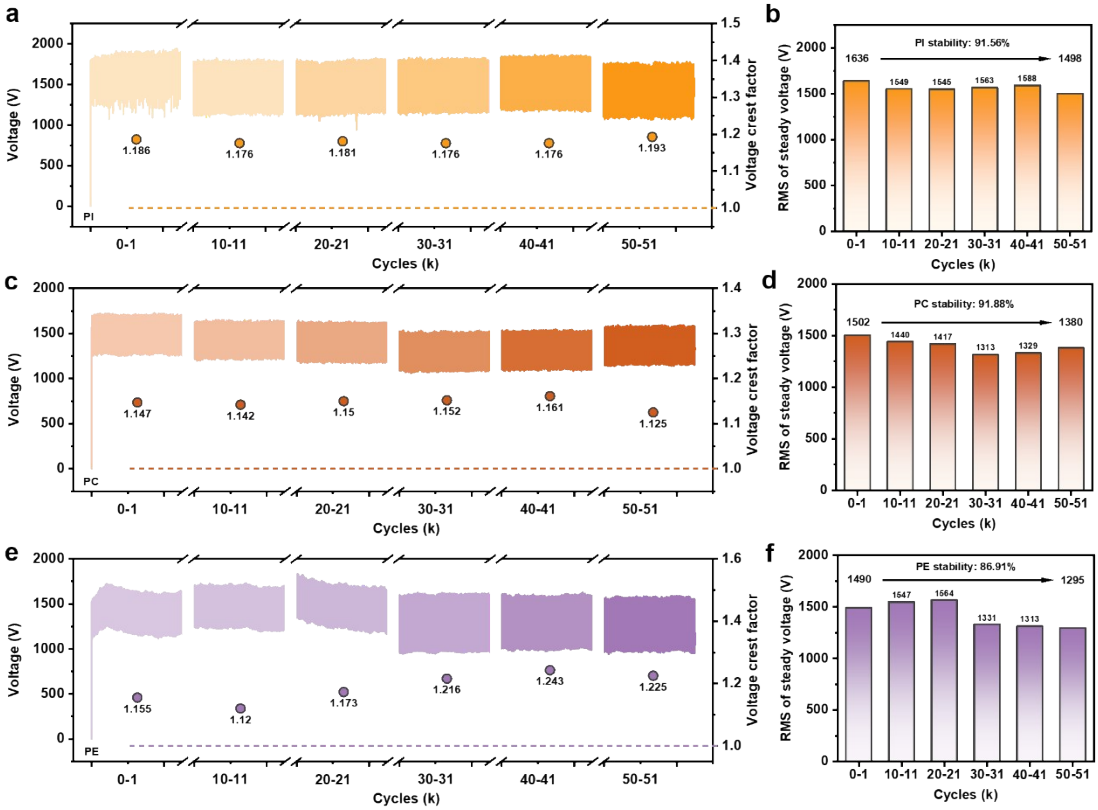

Fig. S6. Stability test of T-DC-TENG with different intermediate triboelectric materials (PI, PC, and PE) within 50000 cycles. Voltage output, RMS of steady voltage, and voltage crest factor of T-DC-TENG with different intermediate triboelectric materials (**a**, **b** PI, **c**, **d** PC, and **e**, **f** PE) per 10000 cycles.

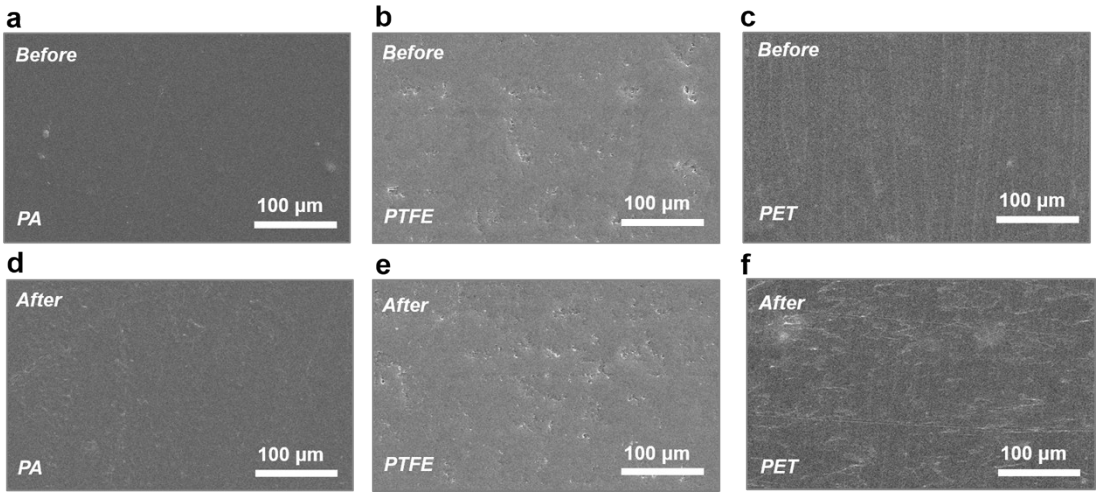

Fig. S7. SEM images of PA, PTFE, and PET films. **a-c** SEM images of PA, PTFE, and PET films before the stability test. **d-f** SEM images of PA, PTFE, and PET films after stability test.

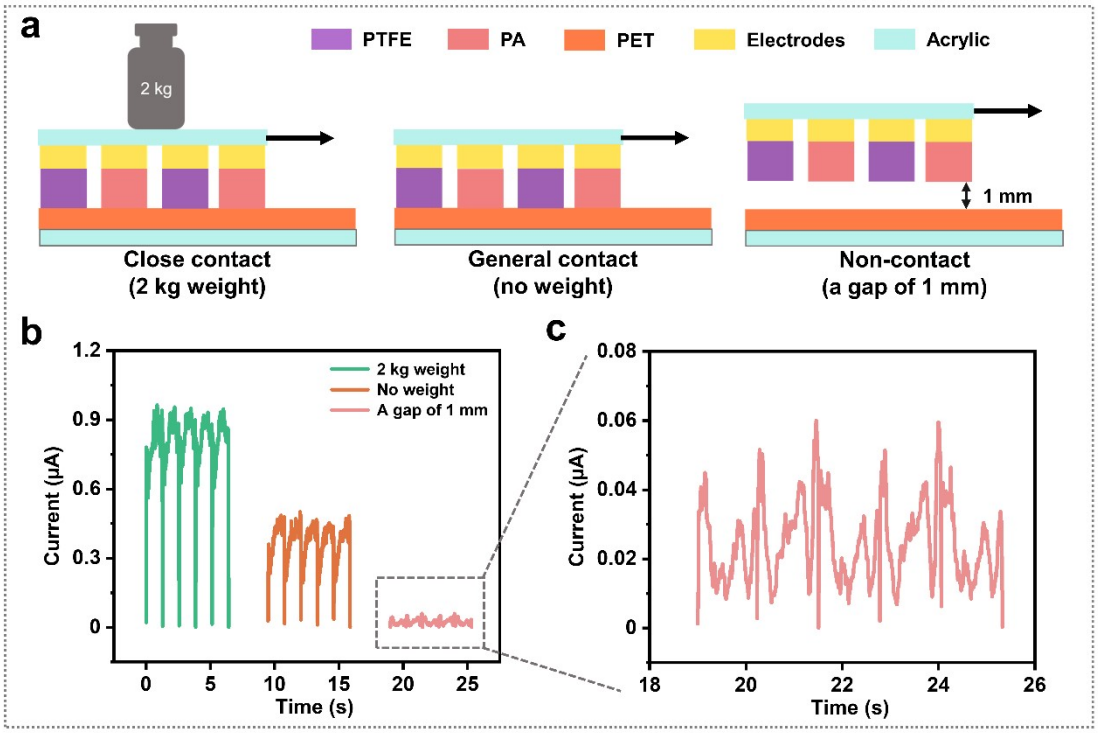

Fig. S8. Effect of different contact modes on output of T-DC-TENG. **a** Schematic diagram of the 2-unit T-DC-TENG testing under the close contact (the slider moves under a weight of 2 kg), general contact (no weight is placed on the slider), and non-contact (there is a 1 mm gap between the slider and the stator). **b** Current output of the 2-unit T-DC-TENG different contact modes.

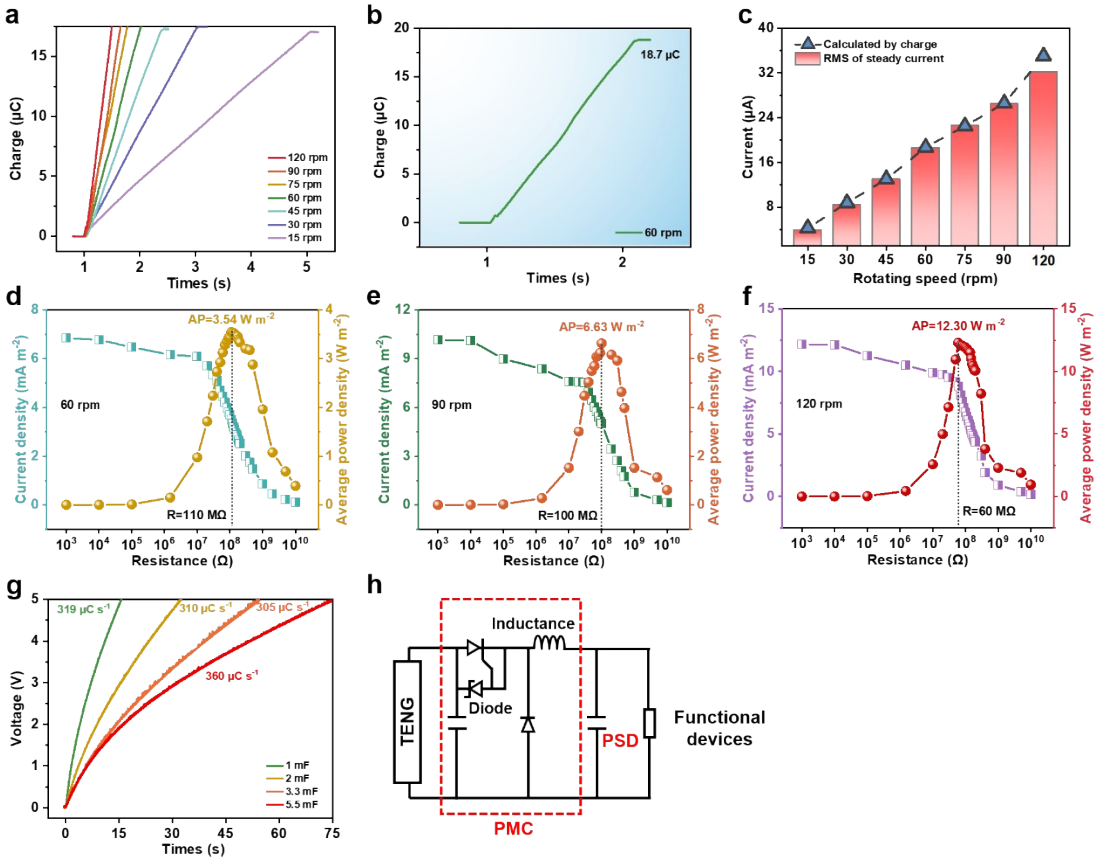

Fig. S9. Performance of 32-unit rotating T-DC-TENG with PET as triboelectric material. **a** Raw data plot of DC output charge of the T-DC-TENG under different rotation speeds. **b** Charge output of the T-DC-TENG at 60 rpm in 1 s. **c** RMS of steady current and current calculated by output charge of the T-DC-TENG under different rotation speeds. **d-f** Matching impendence and average power density of rotary T-DC-TENG at 60 rpm, 90 rpm, and 120 rpm. **g** Charging curves of capacitors (1 mF, 2 mF, 3.3 mF, 5.5 mF) charged by rotary T-DC-TENG at 120 rpm with PMC. The maximum equivalent charging rate of each capacitor charged by T-DC-TENG has been marked. **h** Schematic diagram of PMC.

Supplementary Tables

Table S1. Comparison of the average power density with the latest and most typical DC-TENGs.[1-10]

Article (DC-TENG)	Tribo-materials	Frequency	Area of triboelectric layer (cm^2)	Average power density
Ryu et al Energy Environ. Sci. (2018)[1]	PTFE/PA	15.3 Hz	No	4.9 W m^{-2} 0.32 W m^{-2} Hz^{-1}
Zhou et al Adv. Energy Mater. (2020)[2]	FEP/Cu	0.66 Hz	153.86	0.01072 W m^{-2} Hz^{-1}
Wu et al Nano Energy (2021)[3]	PTFE/Cu	15.8	No	1.225 W m^{-2} 0.078 W m^{-2} Hz^{-1}
Cheng et al Energy Environ. Sci. (2021)[4]	FEP/Cu	1.6 Hz	7.5	0.6 W m^{-2} 0.375 W m^{-2} Hz^{-1}
Wu et al Nat. Commun. (2021)[5]	FEP/PC	1 Hz	No	0.79 W m^{-2} 0.79 W m^{-2} Hz^{-1}
Chen et al Energy Environ. Sci. (2021)[6]	PTFE/Cu/ Rabbit fur	1 Hz	113	1.355 W m^{-2} 1.355 W m^{-2} Hz^{-1}
Li et al Energy Environ. Sci. (2022)[7]	PVC/Cu	8 Hz	706.5	2.032 W m^{-2} 0.254 W m^{-2} Hz^{-1}
Du et al Adv. Funct. Mater. (2022)[8]	FEP/PA	1 Hz	96	2.1 W m^{-2} 2.1 W m^{-2} Hz^{-1}
Li et al Adv. Energy Mater. (2023)[9]	PTFE/ Polyester fur/ PA	2.5 Hz	25.655	8.77 W m^{-2} 3.51 W m^{-2} Hz^{-1}
Zeng et al Adv. Mater. (2023)[10]	PTFE/PU	1 Hz	16	0.398 W m^{-2} Hz^{-1}
This work	PTFE/ PET/ PA	2 Hz	26.267	12.3 W m^{-2} 6.15 W m^{-2} Hz^{-1}

Table S2. Output charge density of the 2-unit T-DC-TENG with different intermediate triboelectric materials.

Materials (2-unit device)	Frication area ($\times 10^{-3}$ m^2)	Average output charge ($\times 10^{-6}$ C)	Output charge density (mC m^{-2})
PE	4.8 (Sliding distance: 10 cm)	0.0819	0.0171
PC	4.8 (Sliding distance: 10 cm)	0.253	0.0527
PI	4.8 (Sliding distance: 10 cm)	0.286	0.0596
PVDF	4.8 (Sliding distance: 10 cm)	0.289	0.0602
PEI	4.8 (Sliding distance: 10 cm)	0.306	0.0638
PVC	4.8 (Sliding distance: 10 cm)	0.411	0.0856
PPS	4.8 (Sliding distance: 10 cm)	0.463	0.0965
PF	4.8 (Sliding distance: 10 cm)	0.530	0.110
PU	4.8 (Sliding distance: 10 cm)	0.542	0.113
PEEK	4.8 (Sliding distance: 10 cm)	0.581	0.121
PP	4.8 (Sliding distance: 10 cm)	0.873	0.182
PET	4.8 (Sliding distance: 10 cm)	0.960	0.2

Table S3. Real-time temperature values recording of each intermediate material in 5 cycles.

Materials	Temperature values (°C)				
PET	**28.7**	**28.8**	**28.8**	**28.9**	**29**
PP	**39.3**	**39.4**	**38.9**	**38.5**	**37.6**
PEEK	**34.8**	**35.1**	**34.5**	**34.1**	**34.4**
PU	**29.8**	**29.9**	**29.9**	**29.6**	**29.6**
PF	**26.7**	**26.7**	**26.7**	**26.7**	**26.8**
PPS	**32.9**	**32.1**	**32.1**	**31.7**	**31.6**
PVC	**32.5**	**32.2**	**32.2**	**32.7**	**32.7**
PEI	**33.7**	**33.5**	**33.2**	**32.7**	**32.7**
PVDF	**36.4**	**36.8**	**36.8**	**36.2**	**34.9**
PI	**30.2**	**29.9**	**29.8**	**30**	**29.8**
PC	**34.3**	**34.3**	**34**	**34**	**33.6**
PE	**35.1**	**34.1**	**34.4**	**34.4**	**34.1**

Table S4. Comprehensive comparison of the 2-unit T-DC-TENG with different intermediate triboelectric materials.

Materials	σ_{DC} (DC output charge density) (mC m^{-2})	μ (friction coefficient)	r (charge retention)	S (stability)	CF (crest factor)	V (RMS of steady voltage) (V)	T (temperature) (°C)
PET	**0.2**	**0.1725**	**90.52%**	**99.72%**	**1.069**	**3572**	**28.8**
PP	**0.182**	**0.19**	**92.3%**	**84.9%**	**1.132**	**2586**	**38.8**
PEEK	**0.121**	**0.235**	**81.87%**	**82%**	**1.189**	**2224**	**34.6**
PU	**0.113**	**0.378**	**48.08%**	**58%**	**1.174**	**1734**	**29.8**
PF	**0.11**	**0.3155**	**8.76%**	**99.9%**	**1.107**	**3100**	**26.7**
PPS	**0.0965**	**0.206**	**84.61%**	**90%**	**1.167**	**2088**	**32.1**
PVC	**0.0856**	**0.28**	**96.88%**	**99.79%**	**1.19**	**1881**	**32.1**
PEI	**0.0638**	**0.165**	**95.64%**	**92.07%**	**1.089**	**1892**	**33.2**
PVDF	**0.0602**	**0.1955**	**65.27%**	**90.77%**	**1.156**	**1475**	**36.2**
PI	**0.0596**	**0.1795**	**64.42%**	**91.56%**	**1.193**	**1498**	**29.9**
PC	**0.0527**	**0.303**	**25.72%**	**91.88%**	**1.125**	**1380**	**34.04**
PE	**0.0171**	**0.247**	**81.96%**	**86.91%**	**1.225**	**1295**	**34.4**

Table S5. Normalized indexes for the comprehensive comparison of the 2-unit T-DC-

TENG with different intermediate triboelectric materials.

Materials	σ^*	$\frac{1}{\mu^*}$	r^*	S^*	$\frac{1}{CF^*}$	V^*	$\frac{1}{T^*}$
PET	**1**	**0.9565**	**0.9052**	**0.9972**	**0.9355**	**1**	**0.9271**
PP	**0.91**	**0.8684**	**0.923**	**0.849**	**0.8834**	**0.724**	**0.6861**
PEEK	**0.605**	**0.7021**	**0.8187**	**0.82**	**0.841**	**0.6226**	**0.7717**
PU	**0.565**	**0.4365**	**0.4808**	**0.58**	**0.8518**	**0.4854**	**0.896**
PF	**0.55**	**0.523**	**0.0876**	**0.999**	**0.9033**	**0.8679**	**1**
PPS	**0.4825**	**0.801**	**0.8461**	**0.9**	**0.8569**	**0.5845**	**0.8318**
PVC	**0.428**	**0.5893**	**0.9688**	**0.9979**	**0.8403**	**0.5266**	**0.8318**
PEI	**0.319**	**1**	**0.9564**	**0.9207**	**0.9183**	**0.5297**	**0.8042**
PVDF	**0.301**	**0.844**	**0.6527**	**0.9077**	**0.8651**	**0.4129**	**0.7376**
PI	**0.298**	**0.9192**	**0.6442**	**0.9156**	**0.8382**	**0.4194**	**0.893**
PC	**0.2635**	**0.5446**	**0.2572**	**0.9188**	**0.8889**	**0.3863**	**0.7844**
PE	**0.0855**	**0.668**	**0.8196**	**0.8691**	**0.8163**	**0.3625**	**0.7762**

Table S6. Slider size with different numbers of units.

Number of units	2	3	4	5	6
Number of electrodes	4	6	8	10	12
Length of electrodes (mm)	10	7	5	4	3.3
Width of electrodes (mm)	48	48	48	48	48
Distance between adjacent electrodes (mm)	1.8	1.11	1.09	1.02	1.2

Table S7. Voltage crest factor of the sliding T-DC-TENG with different numbers of units.

Number of units	Peak voltage (V)	Root mean square of steady voltage (V)	Crest factor
2	4006.12	3329.28	1.20
3	3536.97	3008.83	1.18
4	3411.89	3137.48	1.09
5	3317.28	2911.97	1.14
6	3092.94	2890.6	1.07

Table S8. Systematic comparison of the output charge density with the latest and most

typical works.[2,6-13]

Article (rotation mode)	Type	Frequency	Area of triboelectric layer (cm^2)	Charge output	Charge density per round
Liu et al Sci. Adv. (2019)[11]	Electrostatic discharge	10 Hz	314	1.781 μC/r	0.057 mC m^{-2}
Zhou et al Adv. Energy Mater. (2020)[2]	Electrostatic discharge	1 Hz	153.86	3.5 μC/r	0.227 mC m^{-2}
Zhao et al Nat. Commun. (2020)[12]	Electrostatic discharge	10 Hz	25.133	6.67 μC/r	2.65 mC m^{-2}
Chen et al Energy Environ. Sci. (2021)[6]	Phase control	5 Hz	113.1	4.252 μC/r	0.376 mC m^{-2}
Li et al Energy Environ. Sci. (2022)[7]	Phase control	1 Hz	706.5	14 μC/r	0.198 mC m^{-2}
He et al Adv. Energy Mater. (2022)[13]	Electrostatic discharge	0.167 Hz	209.47	43.8 μC/r	2.09 mC m^{-2}
Du et al Adv. Funct. Mater. (2022)[8]	Mechanical time-delay switch	1 Hz	96	25 μC/r	2.604 mC m^{-2}
Li et al Adv. Energy Mater. (2023)[9]	Ternary dielectric triboelectrification effect	2.5 Hz	25.655	10.01 μC/r	3.902 mC m^{-2}
Zeng et al Adv. Mater. (2023)[10]	Electrostatic discharge	1 Hz	157	9 μC/r	0.573 mC m^{-2}
This work	Ternary dielectric triboelectrification effect and charge leakage	2 Hz	26.267	18.7 μC/r	7.12 mC m^{-2}

Table S9. Current crest factor of rotating T-DC-TENG with PET as triboelectric

material at different rotating speeds.

Rotating speed (rpm)	Peak current (μA)	Root mean square of steady current (μA)	Crest factor
15	4.44	3.93	1.1298
30	9.46	8.43	1.1222
45	14.04	13.02	1.0783
60	18.93	18.61	1.0172
75	22.85	22.62	1.0102
90	26.71	26.48	1.0087
120	32.33	32.19	1.0043

Table S10. Comparison of the crest factor with the representative DC-TENGs.[1-3,6-10] It

is worth noting that the crest factor here is obtained by the ratio of the peak current to the RMS current above.

Article (DC-TENG)	Type	Crest factor
Ryu et al ***Energy Environ. Sci.*** **(2018)[1]**	**Phase control**	**1.26**
Zhou et al ***Adv. Energy Mater.*** **(2020)[2]**	**Electrostatic discharge**	**1.2 (200 rpm)**
Wu et al ***Nano Energy*** **(2021)[3]**	**Phase control**	**1.09**
Chen et al ***Energy Environ. Sci.*** **(2021)[6]**	**Phase control**	**1.05**
Li et al ***Energy Environ. Sci.*** **(2022)[7]**	**Phase control**	**1.03**
Du et al ***Adv. Funct. Mater.*** **(2022)[8]**	**Mechanical time-delay switch**	**1.492**
Li et al ***Adv. Energy Mater.*** **(2023)[9]**	**Ternary dielectric triboelectrification effect**	**1.0082**
Zeng et al ***Adv. Mater.*** **(2023)[10]**	**Electrostatic discharge**	**1.1**
This work	**Ternary dielectric triboelectrification effect and charge leakage**	**1.0043**

Table S11. Voltage crest factor of rotating T-DC-TENG with PET as triboelectric material at different rotating speeds.

Rotating speed (rpm)	Peak voltage (V)	Root mean square of steady voltage (V)	Crest factor
15	3142.49	3057.06	1.0279
30	3009.61	2962.81	1.0158
45	3050.35	3004.23	1.0154
60	3061.21	3027.91	1.0110
75	3067.31	3039.94	1.0090
90	3062.96	3038.16	1.0082
120	3061.09	3040.93	1.0066

Table S12. Comparison of energy conversion efficiency with the latest and most representative rotary TENG.[14-19]

Article (rotary TENG)	Type (AC/DC)	Rotation speed	Energy conversion efficiency η
Zhu et al Nat. Commun. (2021)[14]	Rotary TENG (AC)	3000 rpm	24%
Ding et al *Nano Energy* (2021)[15]	A Schottky DC generator (DC)	0.17 Hz	27.29%
Cho et al *Nano Energy* (2022)[16]	Hybrid generator based on TENG and EMG (AC)	500 rpm	8.75%
Li et al *Appl. Energy* (2022)[17]	Breeze-driven TENG (AC)	4 m s^{-1}	12.06%
Han et al *Adv. Funct. Mater.* (2022)[18]	Rabbit fur-based soft-contact TENG (AC)	6 m s^{-1}	15.4%
He et al *Research* (2022)[19]	Liquid lubrication promoted TENG (AC)	60 rpm	48.61%
This work	Ternary DC-TENG (DC)	120 rpm	22.84%

Supplementary Notes

Note S1: Working mechanism of the sliding T-DC-TENG before reaching charge saturation state.

When the slider slides to the right, due to triboelectrification, PTFE gets electrons and material X loses electrons on the left side of the slider, while material X gains electrons and PA loses electrons on the right side of the slider (**Fig. S1a**). The slider slides forward to leave its original position, and electrostatic induction occurs immediately afterwards (**Fig. S1b**). The back electrode of PA induces negative charges, and the back electrode of PTFE induces positive charges, resulting in a constant current in the external circuit. In **Fig. S1c**, continuous sliding causes PTFE to move above the material X that has rubbed with PA. Since the electronegativity of PTFE is stronger than that of material X, the triboelectric effect ensures that the electrons on material X are "transferred" to PTFE. Frankly speaking, at this time, PTFE and PA respectively have triboelectric effect with material X. Then, electrostatic induction occurs again on the back electrodes of PA and PTFE, and the external circuit produces a current output with the same direction (**Fig. S1d**).

Note S2: The calculation of friction coefficient.

The friction coefficient (μ) of the intermediate triboelectric materials is calculated as follow:

$$\mu = \frac{F_A}{F_G} \tag{1}$$

where F_A is the average value of the traction force measured by the connected digital force gauge when the slider is pulled by a linear motor and slides at a uniform horizontal speed on the stator. F_G is the supporting force of the stator on the slider, which is approximately equal to the weight of the weight on the slider. As shown in **Fig. S2f**, the friction coefficient is obtained by friction between the slider (made of PTFE and PA films) and the intermediate triboelectric material.

Note S3: The equivalent physical model of the T-DC-TENG.

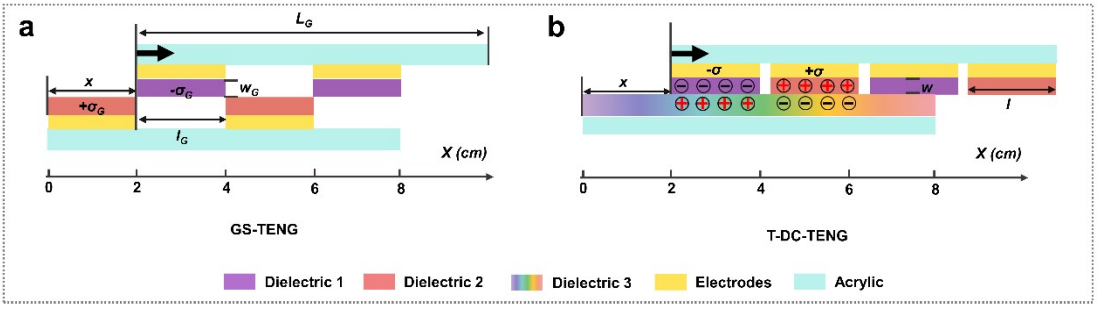

Fig. N1. The equivalent physical model of the T-DC-TENG. **a** Structure and parameter settings of grating structured TENGs with grating electrodes. **b** Theoretical analysis of T-CD-TENG.

As shown in Fig. N1a, the T-DC-TENG is equivalent to the common grating structure TENG of equal plate length (GS-TENG).[9,20] The approximate analytical solution of the Q_{SC-G} of GS-TENG is deduced as follows:

$$Q_{SC-G}=\begin{cases}2w_G x\sigma_G, & 0\le x\le l_G\\ \sigma_G w_G(3l_G-x), & l_G\le x\le 2l_G\\ \sigma_G w_G(l_G-x), & 2l_G\le x\le 3l_G\\ 2w_G l_G\sigma_G, & 3l_G\le x\le 4l_G\end{cases} \tag{2}$$

where σ_G is the triboelectric charge surface density of the dielectric 1, w_G is the width of dielectrics, and l_G is the half-pitch of the GS-TENG. n_G is the number of grating units in the top plate. The total length of the top plate of the GS-TENG is L_G, such that $L_G=2n_G l_G$.[20] In Fig. N1b, l is the half-pitch of the T-DC-TENG. n is the number of units on a certain area of the slider. The total length of the slider of the T-DC-TENG is L, such that $L=2nl$. During sliding, when $0\le x\le l$ and $n=2$, the approximate analytical solution of the Q_{SC-2} of the 2-unit T-DC-TENG is similar to that of GS-TENG.[20]

$$Q_{SC-2}=2wx\sigma \tag{3}$$

where w and σ are the width and triboelectric charge surface density of dielectrics in the T-DC-TENG. During the cyclic motion, the charge always accumulates in one direction spontaneously, forming a DC output. Therefore, when the sliding distance of the slider exceeds l, the accumulated charge (Q_{SC}) of the T-DC-TENG continues to

increase on the charge obtained after each slip. It can be deduced that the Q_{SC} of T-DC-TENG under the short-circuit condition is related to n on a fixed area slider as follows.[9]

$$Q_{SC} = nwx\sigma \tag{4}$$

From the above formula, it can be concluded that the output charge density increases linearly with the increase of n, as shown in **Fig. 3e**. According to $I = \frac{dQ}{dt}$, the current of T-DC-TENG also increases with the number of units.

Note S4: Calculation process of energy conversion efficiency of T-DC-TENG.

According to the energy conversion efficiency formula introduced in the previously reported paper, the energy conversion efficiency η can be described as follow.[19]

$$\eta = \frac{W}{E_f + W + E_r} \tag{5}$$

where W is the output electricity in one rotation, E_f is the energy used to against the friction in one rotation, and E_r is the rotational kinetic energy. The W and E_r are described as follow.

$$W = P_a \cdot t \tag{6}$$

$$E_r = \frac{1}{2}I\omega^2 = \frac{1}{4}m(R_1^2 + R_2^2)\omega^2 \tag{7}$$

where P_a is the average power and t is the time for one rotation. And I is the rotational inertia, ω is the angular velocity, R_1 and R_2 are the inner and outer radius of the rotor.

During the rotation of the turntable, the radius r is perpendicular to the friction force f. Friction moment M is written as follow.

$$M = \int r \times df = \int rdf = \int r\mu dF_N = \frac{2}{3}\mu F_N \frac{R_2^3 - R_1^3}{R_2^2 - R_1^2} \tag{8}$$

$$E_f = \int_0^{2\pi} Md\theta = \frac{4}{3}\mu F_N \frac{R_2^3 - R_1^3}{R_2^2 - R_1^2} \tag{9}$$

Where μ is the dynamic friction coefficient, F_N is the positive pressure, θ is the rotation angle. Therefore, the energy conversion efficiency η is calculated as follows.

$$\eta = \frac{W}{E_f + W + E_r} = \frac{P_a \cdot t}{\frac{4}{3}\mu F_N \frac{R_2^3 - R_1^3}{R_2^2 - R_1^2} + P_a \cdot t + \frac{1}{4}m(R_1^2 + R_2^2)\omega^2} \tag{10}$$

For one rotation of the rotating T-DC-TENG at 120 rpm, P_a is 32.31 mW, t is 0.5 s, μ is 0.1754, F_N is 20 N, R_1 is 10 mm, R_2 is 100 mm, m is 100 g, and ω is 4π. Therefore, after the above calculation, the energy conversion efficiency η of T-DC-TENG is 22.84%.

Supplementary References

1 H. Ryu, J. H. Lee, U. Khan, S. S. Kwak, R. Hinchet and S.-W. Kim, *Energy Environ. Sci.*, 2018, **11**, 2057.

2 L. Zhou, D. Liu, S. Li, Z. Zhao, C. Zhang, X. Yin, L. Liu, S. Cui, Z. L. Wang and J. Wang, *Adv. Energy Mater.*, 2020, **10**, 2000965.

3 Z. Wu, S. Wang, Z. Cao, R. Ding and X. Ye, *Nano Energy*, 2021, **83**, 105787.

4 R. Cheng, K. Dong, P. Chen, C. Ning, X. Peng, Y. Zhang, D. Liu and Z. L. Wang, *Energy Environ. Sci.*, 2021, **14**, 2460-2471.

5 H. Wu, S. Wang, Z. Wang and Y. Zi, *Nat. Commun.*, 2021, **12**, 5470.

6 P. Chen, J. An, R. Cheng, S. Shu, A. Berbille, T. Jiang and Z. L. Wang, *Energy Environ. Sci.*, 2021, **14**, 4523-4532.

7 X. Li, C. Zhang, Y. Gao, Z. Zhao, Y. Hu, O. Yang, L. Liu, L. Zhou, J. Wang and Z. L. Wang, *Energy Environ. Sci.*, 2022, **15**, 1334-1345.

8 Y. Du, S. Fu, C. Shan, H. Wu, W. He, J. Wang, H. Guo, G. Li, Z. Wang and C. Hu, *Adv. Funct. Mater.*, 2022, **32**, 2208783.

9 Q. Li, Y. Hu, Q. Yang, X. Li, X. Zhang, H. Yang, P. Ji, Y. Xi and Z. L. Wang, *Adv. Energy Mater.*, 2023, **13**, 2202921.

10 Q. Zeng, A. Chen, X. Zhang, Y. Luo, L. Tan and X. Wang, *Adv. Mater.*, 2023, **35**, 2208139.

11 D. Liu, X. Yin, H. Guo, L. Zhou, X. Li, C. Zhang, J. Wang and Z. L. Wang, *Sci. Adv.*, 2019, **5**, eaav6437.

12 Z. Zhao, Y. Dai, D. Liu, L. Zhou, S. Li, Z. L. Wang and J. Wang, *Nat. Commun.*, 2020, **11**, 6186.

13 W. He, C. Shan, H. Wu, S. Fu, Q. Li, G. Li, X. Zhang, Y. Du, J. Wang, X. Wang and C. Hu, *Adv. Energy Mater.*, 2022, **12**, 2201454.

14 G. Zhu, J. Chen, T. Zhang, Q. Jing and Z. L. Wang, *Nat. Commun.*, 2014, **5**, 3426.

15 X. Ding, H. Shao, H. Wang, W. Yang, J. Fang, D. Zhang and T. Lin, *Nano Energy*, 2021, **89**, 106367.

16 H. Cho, I. Kim, J. Park and D. Kim, *Nano Energy*, 2022, **95**, 107048.

17 X. Li, Y. Cao, X. Yu, Y. Xu, Y. Yang, S. Liu, T. Cheng and Z. L. Wang, *Appl. Energy*, 2022, **306**, 117977.

18 J. Han, Y. Feng, P. Chen, X. Liang, H. Pang, T. Jiang and Z. L. Wang, *Adv. Funct. Mater.*, 2022, **32**, 2108580.

19 W. He, W. Liu, S. Fu, H. Wu, C. Shan, Z. Wang, Y. Xi, X. Wang, H. Guo, H. Liu and C. Hu, *Research*, 2022, **2022**, 9812865.

20 S. Niu, S. Wang, Y. Liu, Y. S. Zhou, L. Lin, Y. Hu, K. C. Pradel, and Z. L. Wang, *Energy Environ. Sci.*, 2014, **7**, 2339-2349.